IEEE Access
Multidisciplinary | Rapid Review | Open Access Journal

SPECIAL SECTION ON POSITIONING AND NAVIGATION IN CHALLENGING ENVIRONMENTS

Received December 2, 2021, accepted December 8, 2021, date of publication December 13, 2021,
date of current version December 30, 2021.

Digital Object Identifier 10.1109/ACCESS.2021.3135012

Evaluating Tracking Rotations Using Maximal Entropy Distributions for Smartphone Applications

JAMES BROTCHIE[1], WENCHAO LI[1], ALLISON KEALY[1], AND BILL MORAN[2], (Member, IEEE)
[1]Department of Geospatial Science, RMIT University, Melbourne, VIC 3000, Australia
[2]Department of Electrical Engineering, The University of Melbourne, Melbourne, VIC 3010, Australia
Corresponding author: James Brotchie (s3238455@student.rmit.edu.au)

ABSTRACT Recursive attitude estimation of a rigid body from inertial measurements is a crucial component of many modern systems and as such, has a rich historical background of proposed techniques. Recent work has been done on tracking rotations using maximal entropy distributions. However, there has been no evaluation done on the performance of this approach using real inertial data. In this work, we investigate the performance and limitations of classical and modern probabilistic Bayesian approaches and provide a rigorous comparison to attitude estimation on the special rotation group $\mathcal{SO}(3)$ using maximal entropy distributions. The extended Kalman Filter and the unscented Kalman filter are derived as benchmarks in attitude estimation from low-cost inertial measurement units, commonly found in smartphones. To evaluate robustness over multiple sampling intervals, we generated synthetic directional inertial measurements from a typical low-cost 3-axes inertial measurement unit and use the Frobenius Norm as our primary metric. To further our evaluation, we took advantage of a publicly available dataset where inertial measurements are recorded from a number of off-the-shelf smartphones and the ground truth is calculated using a Motion Capture system. Our experiments demonstrate that tracking rotations using maximum entropy distributions produce a more accurate and robust solution in contrast to alternate proven Kalman approaches.

INDEX TERMS Attitude estimation, extended Kalman filter, inertial measurement unit, rotation group, unscented Kalman filter.

I. INTRODUCTION

The ability to accurately and recursively estimate the attitude of a rigid body is a key component in many applications, including aerial, autonomous and subaquatic navigation [1], satellite control and space junk estimation [2], [3], as well as augmented reality and tracking of human and animal body motions [4]. Due to its vast range of applications, it has been the subject of extensive research. Over the years, numerous classic nonlinear estimation algorithms have been put forward to address dynamic state estimation in a nonlinear system and an exhaustive summary of these approaches is given in [5]. Many of the techniques described are computationally complex and particular to a certain device or application. The major issue with nonlinear filters is real time computational complexity to provide a given estimation accuracy. Real time computational complexity depends on several factors, which are explained in [6]. In this work we look at algorithms that are on the order of d^3 for estimating state vectors of dimension d. Additionally, we look at Bayesian estimators, parameterised by rotation matrices that derive attitude perturbation states in the filter. This is due to Bayesian estimators being advantageous in their complete stochastic property definition given by the probability density of the estimated attitude, particularly the level of confidence [7].

Attitude estimation algorithms typically rely on directional measurements acquired, for example, from an inertial measurement unit (IMU). Advancements in micro-electromechanical technologies have allowed for enough processing power in present-day mobile and tablet devices to accommodate an increasing number of sensors. Consumer grade IMUs availability, low-cost, and low power

The associate editor coordinating the review of this manuscript and approving it for publication was Pinjia Zhang.

requirements enable such devices to facilitate real-time applications and navigation solutions [8], [9].

In this paper we focus on Bayesian estimation algorithms that use tri-axial measurements from 3 inertial sensors, commonly found in smartphones. These embedded sensors make it possible to leverage the continuously provided information to estimate the attitude of the rigid sensor body with respect to the Earth's local frame. These IMUs typically consist of a tri-axis accelerometer, gyroscope and magnetometer. The magnetometer and accelerometer provide noisy directional measurements with respect to the Earth's polar North and gravitational acceleration. The gyroscope provides noisy measurements of angular velocity. Directional vector observations can be taken from accelerometer and magnetometer, whereas the gyroscope provides angular velocities. Integration of the angular velocity measurements unfortunately leads to increasingly large errors in attitude estimation due to the sensor bias. A more in depth description of these sensors and their calibrations is provided in [8]. The modelling of the accelerometers, rate gyroscopes and magnetometers take into account the several biases and noise imperfections found in smartphones. An in depth look into a wide range of IMUs and their deficiencies can be found in [10].

As the integration of gyroscope measurements yields poor estimations, accelerometer and magnetometer measurements are used to update error calculations and compensate for the drift. The generalised problem for attitude estimation from IMUs is in the combination of these sensors to provide an optimal solution in the form of an optimal state estimator. Optimal state estimators have been proposed where measurements are mixed with both kinematic and dynamic models [5], [8], [9]. Most of the complexity in attitude estimation lies in the nonlinearity of attitude change and as such requires a non linear estimator. Previous work on attitude estimation with smartphones in [8] and [9], has provided a number of state-of-the-art nonlinear estimators in this space that fit our computational complexity requirements.

The non linear state estimators looked at in this work are: the extended Kalman filter (EKF), the unscented Kalman filter (UKF) and tracking attitude using maximum entropy distributions on the rotation group $\mathcal{SO}(3)$, developed by *Suvorova et al. [11]* - henceforth referred to as the $\mathcal{SO}(3)$ filter. We generated synthetic IMU measurements at varying sampling rates and utilise the publicly available *OXIOD* smartphone dataset [12] to thoroughly compare and contrast each estimation solution. Improving our state estimation from consumer IMUs could promote significant advances in practical applications such as indoor navigation and localisation, inertial odometry and augmented/virtual reality, amongst others. The major contribution of this paper is to provide a rigorous comparative evaluation of attitude estimation algorithms in literature in contrast to tracking rotations using maximal entropy distributions in terms of robustness and accuracy.

The rest of the paper is arranged as follows: the background fundamentals of attitude estimation from IMU data via an EKF, UKF or $\mathcal{SO}(3)$ filter used in this work is given in Section II. Detailed mathematical descriptions are given in Section III, IV and V for the respective filters. The experimental results are presented in Section VI alongside a discussion. Finally, we draw some conclusions and delineate potential future work in Section VII.

II. BACKGROUND

A Kalman-based filter has long been the *de facto* standard for attitude estimation algorithms and their commercial applications [5]. The extended Kalman filter (EKF) was the pioneering real-time attitude estimator and its inception proved integral in live spacecraft attitude estimation [2], [3]. The pervasiveness of the EKF solution is a testament to its effectiveness, however, there are a number of disadvantages.

To account for the nonlinear aspects of rotational kinematics, the EKF predicts the states of the system under the assumption that its observation model and process model are locally linear and then expands upon these using Jacobians. Since the rotation group on $\mathcal{SO}(3)$ has three dimensions, most attitude determining EKFs use lower-dimensional parameterisations [5], [13]. The low dimensionality can lead to implementation difficulty when expanding the Jacobians, as certain attitudes are singular or discontinuous. These singularities cause the EKF error covariance matrix to shrink rapidly in size. Once this matrix is sufficiently small, the EKF has to be re-initialised, causing the estimations to drift over time [3], [5], [14]. Additionally, the calculation of the Jacobian matrix in an EKF is a cumbersome process and is not guaranteed to exist or may not have a finite value [15]. Quaternion based filters have been developed to overcome some deficiencies [2], [16], as quaternion based parameterisations do not exhibit singularities in representing attitude.

Several extensions have been built on the framework of the EKF - most notably the unscented Kalman filter. The UKF is an improvement to the EKF and it generalises the Kalman filter for both linear and nonlinear systems [17]. The UKF builds around the premise that with a fixed number of parameters, approximating a Gaussian distribution should be far simpler than approximating some arbitrary nonlinear function. Introduced in [18], the UKF has been implemented for attitude estimation in [14], [19] with much success. It has several advantages over the EKF, namely a lower expected error as it avoids the derivation of Jacobians as well as being valid for higher order expansions. The UKF uses sigma points to capture the characteristics of a Gaussian distribution. However, the regenerative step of the sigma points can be a major limitation in the propagation of state uncertainty [20].

Alternate estimations for the probabilistic distribution of attitude uncertainty on the manifold have been studied, despite being relatively unpopular in comparison to the aforementioned techniques [7]. Work on attitude estimation on the special orthogonal group is seen in [7], [11], [21]–[24]. In this body of work, the specific form of probability density, the matrix von Mises-Fisher (vMF) distribution, is used to represent the uncertainties in the state estimates. The vMF distribution is defined by 9 parameters when applied to the

special orthogonal group $\mathcal{SO}(3)$ and, as such, is comparable to the Gaussian distribution in $\mathbb{R}^3$, which is completely represented by the three dimensional mean and six dimensional covariance (used in our Kalman variants). We are grateful for Dr Sofia Suvorova's early discussions on the background for this work. Following [11], [23], we use the maximal entropy distributions on the rotation group - the von Mises- Fisher distributions - as a model for the priors in tracking rotations in the $\mathcal{SO}(3)$ filter. To the best of our knowledge, tracking rotations from real inertial measurements in this manner, is absent in literature. This work presents a novel evaluation of tracking rotations using maximum entropy distributions, from real and synthetic inertial measurements. We leverage popular Kalman filters as benchmarks.

III. $\mathcal{SO}(3)$ FILTER

The group of rotations in three dimensions is the special orthogonal group $\mathcal{SO}(3)$. Attitude of an object in three dimensional space can be represented by an element of the special orthogonal group that corresponds to its rotation from some arbitrary initial state. The vMF distribution is the maximal entropy probability over these rotations. Any attitude estimation approach starts with the definition of the state vector that defines the time varying system and then to propagate this state by computing the posterior distribution of the rotating body.

A. MEAN AND CONCENTRATION MATRICES ON $\mathcal{SO}(3)$

The state of the system is represented by a rotation matrix, an element of the special orthogonal group $\mathcal{SO}(3)$, where

$$\mathcal{SO}(3) = \left\{\mathbf{R} \in \mathbb{R}^{3\times 3} | \mathbf{R}^T\mathbf{R} = \mathbf{I}_3; \det[\mathbf{R}] = 1\right\} \tag{1}$$

where $\mathbf{I}_3$ is 3-dimensional identity matrix.

The matrix von-Mises Fisher distribution on $\mathcal{SO}(3)$ is defined as follows.

Definition 1: A random rotation matrix, $\mathbf{R} \in \mathcal{SO}(3)$, is distributed according to a vMF distribution if its probability density function is defined on $\mathcal{SO}(3)$ as

$$p(\mathbf{R}) = p(\mathbf{R}|\mathbf{A}) = \alpha(\mathbf{A}) \operatorname{etr}\left(\mathbf{A}^T\mathbf{R}\right) \tag{2}$$

where $\operatorname{etr}(\cdot) = \exp(\operatorname{tr}(\cdot))$, matrix $\mathbf{A} \in \mathbb{R}^{3\times 3}$, encompasses said location (rotational mean) and measure of spread (concentration) and $\alpha(\mathbf{A}) \in \mathbb{R}$ is the normalization factor such that $\int_{\mathcal{SO}(3)} p(\mathbf{R}; \mathbf{A})[d\mathbf{R}] = 1$. $[dR]$ denotes integration with respect to the Haar measure on Lie group $\mathcal{SO}(3)$. Furthermore, we denote $\mathbf{R} \sim vMF(\mathbf{A})$.

Proposition 1: The product of two matrix vMF distributions can be written into a matrix vMF distribution after normalization, i.e.

$$p(\mathbf{R}; \tilde{\mathbf{A}}) = \beta(\mathbf{A}_1, \mathbf{A}_2) p(\mathbf{R}; \mathbf{A}_1) p(\mathbf{R}; \mathbf{A}_2) \tag{3}$$

where $\beta(\mathbf{A}_1, \mathbf{A}_2)$ is the normalizer.

Proof:

$$\begin{aligned} p(\mathbf{R}; \mathbf{A}_1)p(\mathbf{R}; \mathbf{A}_2) &= \alpha(\mathbf{A}_2) \operatorname{etr}\left(\mathbf{A}_2^T\mathbf{R}\right) \alpha(\mathbf{A}_1) \operatorname{etr}\left(\mathbf{A}_1^T\mathbf{R}\right) \\ &= \alpha(\mathbf{A}_2)\alpha(\mathbf{A}_1) \operatorname{etr}\left((\mathbf{A}_1 + \mathbf{A}_2)^T\mathbf{R}\right) \\ &\triangleq \alpha(\mathbf{A}_2)\alpha(\mathbf{A}_1) \operatorname{etr}\left(\tilde{\mathbf{A}}^T\mathbf{R}\right) \end{aligned}$$

Therefore, there exists $\beta(\mathbf{A}_1, \mathbf{A}_2)$ such that

$$\int_{\mathcal{SO}(3)} \beta(\mathbf{A}_1, \mathbf{A}_2)\alpha(\mathbf{A}_2)\alpha(\mathbf{A}_1) \operatorname{etr}\left(\tilde{\mathbf{A}}^T\mathbf{R}\right) [d\mathbf{R}] = 1 \tag{4}$$

□

The matrix $\mathbf{A}$ can be decomposed as the product $\mathbf{A} = \hat{\mathbf{R}}^T\mathbf{A}_0 = \hat{\mathbf{R}}^T\mathbf{V}\mathbf{\Sigma}\mathbf{V}^T$, see [25], where $\hat{\mathbf{R}}$ is the polar component and $\mathbf{A}_0 = \mathbf{V}\mathbf{\Sigma}\mathbf{V}^T$ is the elliptical component, also known as the concentration matrix. Equivalently, we have $\mathbf{R} \sim \text{vMF}(\hat{\mathbf{R}}^T\mathbf{A}_0)$. It is important to note that if $\mathbf{A}$ is singular, this decomposition may not be unique. Function $\alpha(\mathbf{A})$ can be calculated in terms of an asymmetric version of the hyper-geometric function ${}_0F_1\left(\frac{3}{2}; \frac{1}{4}\mathbf{\Sigma}^2\right)$, where $\mathbf{\Sigma}$ is a matrix of eigenvalues of the concentration matrix.

The first moment is given by

$$\mathbf{E} = \mathbf{V} f(\mathbf{\Sigma}) \mathbf{V}^T \hat{\mathbf{R}}, \tag{5}$$

where $f(\mathbf{\Sigma})$ is a diagonal matrix with entries f_i defined by

$$\frac{\partial}{\partial \kappa_i} \log {}_0F_1\left(\frac{3}{2}; \frac{1}{4}\mathbf{\Sigma}^2\right), \text{ for } i = 1, 2, 3 \tag{6}$$

A closed-form and approximate method to calculate $f(\mathbf{\Sigma})$ can be found in [23].

B. LIKELIHOOD FUNCTION AND PRIOR DENSITY

The Bayesian framework proposed in [23] assumes that the posterior density of the rotation matrix at time k, i.e. $\mathbf{R}_k$, is vMF distributed:

$$p(\mathbf{R}_k|\mathbf{Z}_{k-1}, \cdots, \mathbf{Z}_1) = \alpha(\mathbf{A}_k) \operatorname{etr}\left(\hat{\mathbf{R}}_k^T\mathbf{A}_k\mathbf{R}_{k-1}\right) \tag{7}$$

where $\mathbf{Z}_i$ is the measurement at time i, $\mathbf{A}_k$ is concentration matrix and $\hat{\mathbf{R}}_k^T$ is a mean. Obviously, the $\mathbf{A}_k$ and $\hat{\mathbf{R}}_k^T$ should be dependent on $\mathbf{Z}_k$.

For the state transition, it is assumed that, at time k, the attitude $\mathbf{R}_k$ is transited from $\mathbf{R}_{k-1}$ through another random rotation matrix $\mathbf{P}_k \sim \text{vMF}(\hat{\mathbf{P}}_k^T\mathbf{B}_k)$, where $\hat{\mathbf{P}}_k^T$ is a mean and $\mathbf{B}_k = \mathbf{U}_{\mathbf{B}_k}\mathbf{\Sigma}_{\mathbf{B}_k}\mathbf{U}_{\mathbf{B}_k}^T$ is a concentration matrix of the dynamics. The state dynamics transition probability is then written in terms of the distribution matrix, $\mathbf{P}_k$

$$p(\mathbf{R}_k|\mathbf{R}_{k-1}) = \alpha(\mathbf{B}_k) \operatorname{etr}\left(\hat{\mathbf{P}}_k^T\mathbf{B}_k\mathbf{R}_k\mathbf{R}_{k-1}\right) \tag{8}$$

The prior distribution of $\mathbf{R}_k$ is then given by

$$\begin{aligned} &p(\mathbf{R}_k|\mathbf{Z}_{k-1}, \cdots, \mathbf{Z}_1) \\ &= \int_{\mathcal{SO}(3)} p(\mathbf{R}_k|\mathbf{R}_{k-1}) p(\mathbf{R}_{k-1}|\mathbf{Z}_{k-1}, \cdots, \mathbf{Z}_1)[d\mathbf{R}_{k-1}] \end{aligned} \tag{9}$$

$$\begin{aligned} &= \alpha(\mathbf{B}_k)\alpha(\mathbf{A}_{k-1}) \int_{\mathcal{SO}(3)} \operatorname{etr}\left(\hat{\mathbf{P}}_k^T\mathbf{B}_k\mathbf{R}_k\mathbf{R}_{k-1}\right) \dots \\ &\quad \dots \operatorname{etr}\left(\hat{\mathbf{R}}_{k-1}^T\mathbf{A}_{k-1}\mathbf{R}_{k-1}\right) [d\mathbf{R}_{k-1}] \end{aligned} \tag{10}$$

This resultant integral is intractable and is therefore approximated with a vMF distribution to allow for a recursive process to estimate the attitude over time. Since R_k is assumed to be distributed by a vMF, then its first moment can be estimated as the product of two vMF variates, Eq. (5)

$$\hat{\mathbf{E}}_k = \left(\mathbf{U}_{\mathbf{B}_k} f(\mathbf{\Sigma}_{\mathbf{B}_k}) \mathbf{U}_{\mathbf{B}_k}^T \hat{\mathbf{P}}_k\right) \left(\mathbf{U}_{\mathbf{A}_{k-1}} f(\mathbf{\Sigma}_{\mathbf{A}_{k-1}}) \mathbf{U}_{\mathbf{B}_{k-1}}^T \hat{\mathbf{R}}_{k-1}\right) \tag{11}$$

where $\left(\mathbf{U}_{\mathbf{B}_k} f(\mathbf{\Sigma}_{\mathbf{B}_k}) \mathbf{U}_{\mathbf{B}_k}^T \hat{\mathbf{P}}_k\right)$ corresponds to $\hat{\mathbf{P}}_k^T \mathbf{B}_k$ while $\left(\mathbf{U}_{\mathbf{A}_{k-1}} f(\mathbf{\Sigma}_{\mathbf{A}_{k-1}}) \mathbf{U}_{\mathbf{B}_{k-1}}^T \hat{\mathbf{R}}_{k-1}\right)$ corresponds to $\hat{\mathbf{R}}_{k-1}^T \mathbf{A}_{k-1}$.

Equivalently, (11) can be polar decomposed to

$$\hat{\mathbf{E}}_k = \mathbf{U}_{\mathbf{C}_{k-1}} f(\Sigma_{\mathbf{C}_{k-1}}) \mathbf{U}_{\mathbf{C}_{k-1}}^T \mathbf{Q}_k \tag{12}$$

so we then have the distribution, $\mathbf{R}_k$, approximated by

$$p(\mathbf{R}_k | \mathbf{Z}_{k-1}, \cdots, \mathbf{Z}_1) = \alpha(\mathbf{C}_k) \operatorname{etr}\left(\mathbf{Q}_k^T \mathbf{C}_k \mathbf{R}_k\right) \tag{13}$$

where $\mathbf{Q}_k$ is the mean, $\mathbf{C}_k = \mathbf{U}_{\mathbf{C}_{k-1}} \mathbf{\Sigma}_{\mathbf{C}_{k-1}} \mathbf{U}_{\mathbf{C}_{k-1}}^T$ is the concentration matrix.

To summarise, in order to find the vMF distribution $\mathbf{R} \sim \text{vMF}(\mathbf{R}|\hat{\mathbf{R}}^T \mathbf{A})$ approximating the distribution of a rotation matrix $\mathbf{R}$ w.r.t $\mathbf{Z}$, we first compute the polar decomposition of $\mathbf{Z}$ to obtain the modal matrix $\hat{\mathbf{R}}$.

C. MEASUREMENT MODEL AND BAYESIAN UPDATE STEP

The measurements, $\mathbf{Z}_k$, are assumed to be distributed in accordance with a vMF. As such, the likelihood function at time k is

$$\ell(\mathbf{Z}_k | \mathbf{R}_k) = \alpha(\mathbf{X}\mathbf{M}\mathbf{Z}_k^T) \operatorname{etr}\left(\mathbf{X}\mathbf{M}\mathbf{Z}_k^T \mathbf{R}_k\right) \tag{14}$$

where the matrix $\mathbf{X}$ is columned by the gravity and magnetic reference vectors (in a global coordinate system) and $\mathbf{M}$ is a matrix with diagonals that correspond to the measurement concentration parameters. From Proposition 1, we know that the posterior distribution is still vMF distributed. Specifically, recall the proposed form of the posterior distribution, we have following result via Bayes's rule

$$\begin{aligned} p(\mathbf{R}_k | \mathbf{Z}_k, \mathbf{Z}_{k-1}, \cdots, \mathbf{Z}_1) &\propto \ell(\mathbf{Z}_k | \mathbf{R}_k) p(\mathbf{R}_k | \mathbf{Z}_{k-1}, \cdots, \mathbf{Z}_1) \\ &= \operatorname{etr}\left(\mathbf{X}\mathbf{M}\mathbf{Z}_k^T \mathbf{R}_k + \mathbf{Q}_k^T \mathbf{C}_k \mathbf{R}_k\right) \\ &= \operatorname{etr}\left(\left(\mathbf{X}\mathbf{M}\mathbf{Z}_k^T + \mathbf{Q}_k^T \mathbf{C}_k\right) \mathbf{R}_k\right) \\ &= \operatorname{etr}\left(\hat{\mathbf{R}}_k^T \mathbf{A}_k \mathbf{R}_k\right) \\ \iff \mathbf{R}_k | \mathbf{Z}_k, \mathbf{Z}_{k-1}, \cdots, \mathbf{Z}_1 &\sim \text{vMF}(\hat{\mathbf{R}}_k^T \mathbf{A}_k) \end{aligned} \tag{15}$$

where the new parameters $\hat{\mathbf{R}}_k$ and $\mathbf{A}_k$ are computed as the polar decomposition of matrix $\mathbf{X}\mathbf{M}\mathbf{Z}_k^T + \mathbf{Q}_k^T \mathbf{C}_k$ - as done in Eq. (5).

IV. EXTENDED KALMAN FILTER

An EKF was used to estimate the attitude alongside the $\mathcal{SO}(3)$ Filter. In this section we outline how the filter was built [3], [5], [16], [26]. The rotation of an object in motion can be defined by Euler angles, represented by roll ϕ, pitch θ and yaw ψ. The angular rate is defined by ω_x, ω_y and ω_z along x, y and z axis respectively. We then have

$$\begin{bmatrix} \dot{\phi} \\ \dot{\theta} \\ \dot{\psi} \end{bmatrix} = \mathbf{T}(\phi, \theta, \psi) \begin{bmatrix} \omega_x \\ \omega_y \\ \omega_z \end{bmatrix} \tag{16}$$

where

$$\mathbf{T}(\phi, \theta, \psi) = \begin{bmatrix} 1 & \frac{\mathbf{s}_\phi \mathbf{s}_\theta}{\mathbf{c}_\theta} & \frac{\mathbf{c}_\phi \mathbf{s}_\theta}{\mathbf{c}_\theta} \\ 0 & \mathbf{c}_\phi & -\mathbf{s}_\phi \\ 0 & \frac{\mathbf{s}_\phi}{\mathbf{c}_\theta} & \frac{\mathbf{c}_\phi}{\mathbf{c}_\theta} \end{bmatrix} \tag{17}$$

and $\mathbf{s}_x = \sin(x)$, $\mathbf{c}_x = \cos(x)$.

Now to construct Kalman filter, the following model is considered

$$\mathbf{x}_k = \begin{bmatrix} \mathbf{v}_k \\ \mathbf{b}_k \end{bmatrix} = \left[\phi_k, \theta_k, \psi_k, b_{x,k}, b_{y,k}, b_{z,k}\right]^T \tag{18}$$

where $\mathbf{v}_k = [\phi_k, \theta_k, \psi_k]^T$ and $\mathbf{b}_k = \left[b_{x,k}, b_{y,k}, b_{z,k}\right]^T$ is the gyro bias. Therefore, the states $\mathbf{x}_k = [\mathbf{v}_k, \mathbf{b}_k]^T$ at time k are

$$\mathbf{v}_k = \mathbf{v}_{k-1} + \mathbf{T}_{k-1} \left(\mathbf{u}_{k-1} - \mathbf{b}_{k-1}\right) \Delta t \tag{19}$$

$$\mathbf{b}_k = \mathbf{b}_{k-1} \tag{20}$$

where $\mathbf{T}_k = \mathbf{T}(\mathbf{v}_k)$ and $\mathbf{u}_k$ is the gyro measurement. The transition model is

$$\mathbf{x}_k = g(\mathbf{x}_{k-1}, \mathbf{u}_{k-1}) + \mathbf{w}_{k-1} \tag{21}$$

where $g(\cdot)$ is the nonlinear function defined in (19) and (20) and $\mathbf{w}_k$ is the noise term with mean zero and covariance $\mathbf{Q}$.

The measurement model is

$$\mathbf{z}_k = h(\mathbf{x}_k, \mathbf{v}_k) = \begin{bmatrix} \mathbf{R}_k^T \mathbf{r}_a \\ \mathbf{R}_k^T \mathbf{r}_m \end{bmatrix} + \mathbf{v}_k \tag{22}$$

where $h(\cdot)$ is the nonlinear function, $\mathbf{R}_k^T$ is rotation matrix, $\mathbf{r}_a$ and $\mathbf{r}_m$ are nominal gravitational acceleration and magnetic field vector, and $\mathbf{v}_{k+1}$ is Gaussian noise term with mean zero and covariance $\mathbf{C}$.

The EKF is therefore given by

$$\begin{aligned} \hat{\mathbf{x}}_{k|k-1} &= g(\hat{\mathbf{x}}_{k-1}, \mathbf{u}_{k-1}) \\ \mathbf{B}_{k|k-1} &= \mathbf{A}_{k-1} \mathbf{B}_{k-1|k-1} \mathbf{A}_{k-1}^T \mathbf{Q}_{k-1} \\ \mathbf{S}_k &= \mathbf{H}_k \mathbf{B}_{k|k-1} \mathbf{H}_k^T + \mathbf{M}_k \mathbf{C} \mathbf{M}_k^T \\ \mathbf{K}_k &= \mathbf{B}_{k|k-1} \mathbf{H}_k^T \left(\mathbf{H}_k \mathbf{B}_{k|k-1} \mathbf{H}_k^T + \mathbf{C}_k\right)^{-1} \\ \hat{\mathbf{x}}_{k|k} &= \hat{\mathbf{x}}_{k|k-1} + \mathbf{K}_k \left(\mathbf{z}_k - h\left(\hat{\mathbf{x}}_{k|k-1}\right)\right) \\ \mathbf{B}_{k|k} &= \left(\mathbf{I} - \mathbf{K}_k \mathbf{H}_k\right) \mathbf{B}_{k|k-1} \end{aligned} \tag{23}$$

where $\mathbf{A}_{k-1} = \frac{\partial g_k}{\partial \mathbf{x}}\Big|_{\hat{\mathbf{x}}_{k-1|k-1}, \mathbf{u}_{k-1}}$, $\mathbf{H}_{k-1} = \frac{\partial h}{\partial \mathbf{x}}\Big|_{\hat{\mathbf{x}}_{k-1|k-1}}$ and $\mathbf{M}_{k-1} = \frac{\partial h}{\partial \mathbf{v}}\Big|_{\hat{\mathbf{x}}_{k-1|k-1}}$.

Remark 1: A visual example to illustrate the main difference between EKF and $\mathcal{SO}(3)$ tracker is shown in Fig. 1. Due to the linearization process of the EKF (left), $\mathbf{A}_{k-1}\mathbf{x}_{k-1}$ is on the tangent plane of point $\mathbf{x}_{k-1}$ and has an error with desired

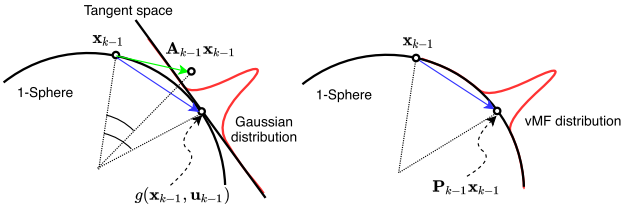

FIGURE 1. A visualisation of the EKF (left) and $\mathcal{SO}(3)$ tracker (right) estimation processes.

$g(\mathbf{x}_{k-1}, \mathbf{u}_{k-1})$, where $g(\mathbf{x}_{k-1}, \mathbf{u}_{k-1})$ is transition model and $\mathbf{A}_{k-1}$ is linearization of function g. Whereas in the $\mathcal{SO}(3)$ tracker (right), the local linearization process is not involved and the distribution is located directly on the unit-sphere.

V. UNSCENTED KALMAN FILTER

The unscented Kalman filter is a powerful tool when the underlying models are nonlinear. Based on the work in [27], we complete the UKF formulation here. The quaternion based UKF can be found in [28].

At time k, the UKF is, $i = 1, \cdots, d$.

$$\boldsymbol{\chi}_{0,k-1|k-1} = \mathbf{x}_{k-1|k-1} \tag{24}$$
$$\Delta\boldsymbol{\chi}_{i,k-1|k-1} = d^{1/2}\mathbf{p}_i \tag{25}$$
$$\boldsymbol{\chi}_{i,k-1|k-1} = \mathbf{x}_{k-1|k-1} + \Delta\boldsymbol{\chi}_{i,k-1|k-1} \tag{26}$$
$$\boldsymbol{\chi}_{i+d,k-1|k-1} = \mathbf{x}_{k-1|k-1} - \Delta\boldsymbol{\chi}_{i,k-1|k-1} \tag{27}$$

where $\mathbf{p}_i$ is i-th column of $\left(\mathbf{P}_{\mathbf{xx},k-1|k-1} + \mathbf{Q}_k\right)^{1/2}$, $\mathbf{P}_{\mathbf{xx},\cdot|\cdot}$ is covariance matrix of $\mathbf{x}_{\cdot|\cdot}$.

Then the weights are

$$w_0 = \frac{1}{d}, \quad w_i = w_{i+d} = \frac{1}{2d} \tag{28}$$

The prediction step and measurement update step are given as follows

$$\begin{aligned}
\mathbf{x}_{k|k-1} &= \sum_{i=0}^{2d} w_i g\left(\boldsymbol{\chi}_{i,k-1|k-1}\right) \\
\mathbf{P}_{\mathbf{xx},k|k-1} &= \sum_{i=0}^{2d} w_i \left(\boldsymbol{\chi}_{i,k|k-1} - \mathbf{x}_{k|k-1}\right)\left(\boldsymbol{\chi}_{i,k|k-1} - \mathbf{x}_{k|k-1}\right)^T \\
\mathbf{y}_{k|k-1} &= \sum_{i=0}^{2d} w_i h\left(\boldsymbol{\chi}_i^{k-1|k}\right) \\
\mathbf{P}_{\mathbf{yy}}^{k|k-1} &= \sum_{i=0}^{2d} w_i \left(h\left(\boldsymbol{\chi}_i^{k-1|k}\right) - \mathbf{y}_{k|k-1}\right)\left(h\left(\boldsymbol{\chi}_i^{k-1|k}\right)\right. \\
&\quad \left. - \mathbf{y}_{k|k-1}\right)^T + \mathbf{C}_k \\
\mathbf{P}_{\mathbf{xy}}^{k|k-1} &= \sum_{i=0}^{2d} w_i \left(\boldsymbol{\chi}_i^{k|k-1} - x_{k|k-1}\right)\left(h\left(\boldsymbol{\chi}_i^{k-1|k}\right)\right. \\
&\quad \left. -\mathbf{y}_{k|k-1}\right)^T
\end{aligned} \tag{29}$$

where $\mathbf{P}_{\mathbf{xy},\cdot|\cdot}$ is covariance matrix of $\mathbf{x}_{\cdot|\cdot}$ and $\mathbf{y}_{\cdot|\cdot}$.

Finally, the correction step is

$$\begin{aligned}
\mathbf{S}_k &= \mathbf{P}_{\mathbf{xy}}^{k|k-1}\left(\mathbf{P}_{\mathbf{yy}}^{k|k-1}\right)^{-1} \\
\mathbf{x}_{k|k} &= \mathbf{x}_{k|k-1} + \mathbf{S}_k\left(\mathbf{z}_k - \mathbf{y}_{k|k-1}\right) \\
\mathbf{P}_{\mathbf{xx}}^{k|k} &= \mathbf{P}_{xx}^{k|k-1} - \mathbf{S}_k\mathbf{P}_{\mathbf{yy}}^{k|k-1}\mathbf{S}_k^T.
\end{aligned} \tag{30}$$

VI. EXPERIMENTS

In this section we illustrate the approaches presented in the previous sections with synthetic and real IMU measurements. The simulated measurements were generated to best mimic a typical IMU found in a modern smartphone, where white gaussian measurement noise standard deviations were given by $0.01G$, 0.1 rad/s and $0.4\mu T$ for each axis of the accelerometer, gyroscope and magnetometer, respectively [29]. Doing this synthetically gives us access to the ground truth over the exact same rotations with the ability to vary our sampling rate. Our experiments involve 1000, 10 second long, Monte-Carlo simulations over multiple sampling rates. The *OXIOD* dataset is used to evaluate each estimation solution on a large set of real world data, comprising of multiple smartphones, users and activities. The combination of experiments were designed to best demonstrate each algorithm's robustness and applicability.

A. ATTITUDE ESTIMATION: SYNTHETIC DATA

The most valuable performance metric in the proposed attitude estimation systems is the estimation error while the sensor is in dynamic motion, where there is no rest time for the filters to reinitialise without compromising the current estimate. We have simulated measurements from IMUs, comprising of a triaxial accelerometer, gyroscope and magnetometer. The simulation was implemented with the following setup: a simultaneous rotation around x and y axis at 6.28 rad/s with the covariance of measurement noise for each respective sensor defined as $\sigma_a = [0.0361, 0.0455, 0.0330]$, $\sigma_g = [0.008, 0.0065, 0.0086]$, $\sigma_m = [0.0011, 0.00098, 0.00098]^T$ [28], and the sampling rate at 10Hz, 100Hz and 1000Hz. The simulation results are shown in Fig. 2 - 10. The Frobenius norm of the differences between reference and estimate are given, as follows

$$\mathrm{L}(t) = 3 - \mathrm{tr}(\hat{\mathbf{R}}(t)\mathbf{R}^T(t)), \tag{31}$$

where t denotes the time, $\hat{\mathbf{R}}(t)$ is the estimates of the attitude at time t and $\mathbf{R}$ is rotation matrix of the reference attitude. These are displayed in Fig. 4, 7 and 10 and provide a visually simple, 3-dimensional performance depiction where $\mathrm{L}(t)$ corresponds to the *closeness* between the attitude estimation and truth.

Figures 2, 3, 5, 6, 8, 9 show how each approach's individual Euler parameter errors and estimates are evaluated through the aggregated simulations. The error plots in Figures 2, 5 and 8 best depict how each approach handles each estimation parameter, and how this progresses as the sampling interval decreases. It follows from the comparison of these figures that the performance of the $\mathcal{SO}(3)$ and UKF are not as sensitive

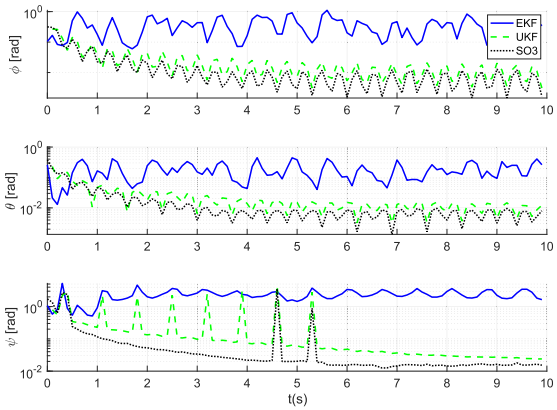

FIGURE 2. (top) Yaw, (middle) pitch and (bottom) roll estimation errors in the EKF, UKF and $\mathcal{SO}(3)$ at 10Hz.

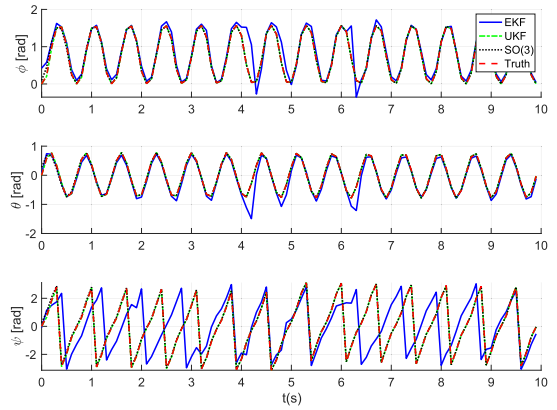

FIGURE 3. (top) Yaw, (middle) pitch and (bottom) roll estimations in the EKF, UKF and $\mathcal{SO}(3)$ at 10Hz.

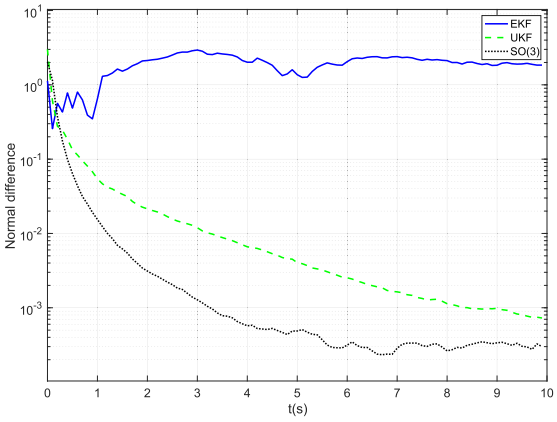

FIGURE 4. Frobenius norm of the EKF, UKF and $\mathcal{SO}(3)$ rotation matrices at 10Hz.

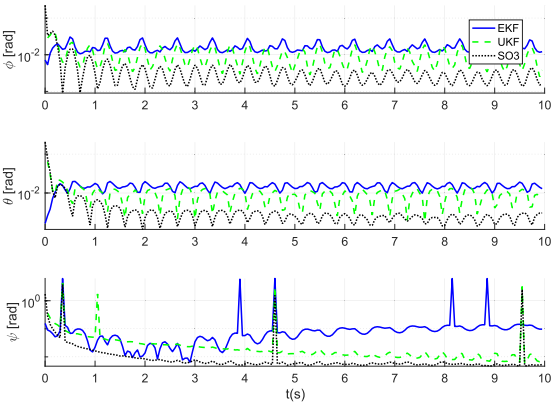

FIGURE 5. (top) Yaw, (middle) pitch and (bottom) roll estimation errors in the EKF, UKF and $\mathcal{SO}(3)$ at 100Hz.

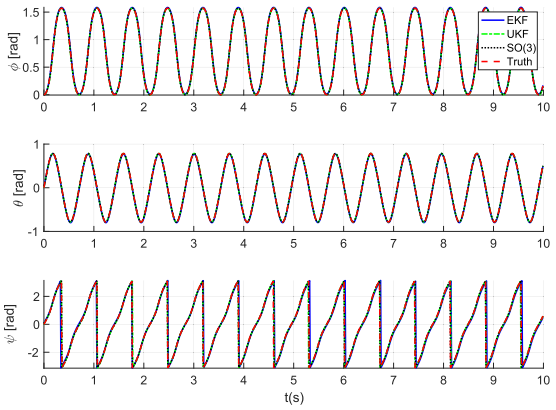

FIGURE 6. (top) Yaw, (middle) pitch and (bottom) roll estimations in the EKF, UKF and $\mathcal{SO}(3)$ at 100Hz.

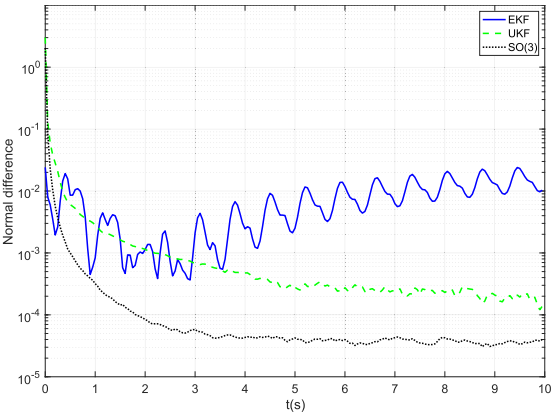

FIGURE 7. Frobenius norm of the EKF, UKF and $\mathcal{SO}(3)$ rotation matrices at 100Hz.

to the measurement frequency as the EKF. The $\mathcal{SO}(3)$ filter clearly separates itself from the Kalman approaches in its yaw estimation, where again we see the EKF struggle to keep up and accumulate errors over time. The average distance in the $\mathcal{SO}(3)$ group between estimate and truth for each filter, L(t), (Figures 4, 7 and 10) provides an easily comprehensible visualisation of performance comparison. From our simulations at 10Hz in Figure 4, it is evident that the process model of the $\mathcal{SO}(3)$ tracker, defined on the sphere directly using a vMF distribution, is advantageous when compared to Kalman process models which are defined on the tangent plane. This is due to the position of the Normal distribution in Euclidean space. As a result, when the time between samples increases,

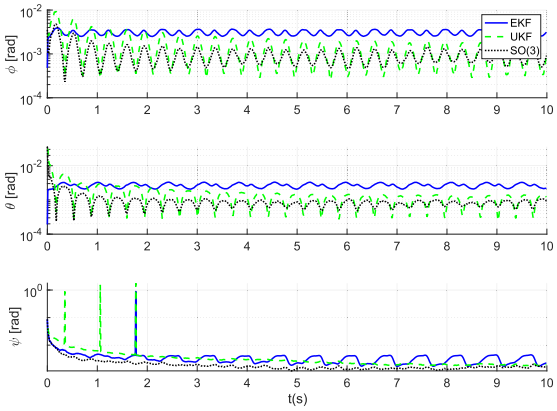

FIGURE 8. (top) Yaw, (middle) pitch and (bottom) roll estimation errors in the EKF, UKF and $\mathcal{SO}(3)$ at 1000Hz.

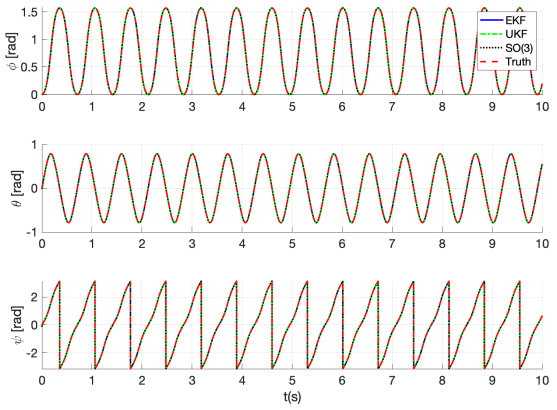

FIGURE 9. (top) Yaw, (middle) pitch and (bottom) roll estimations in the EKF, UKF and $\mathcal{SO}(3)$ at 1000Hz.

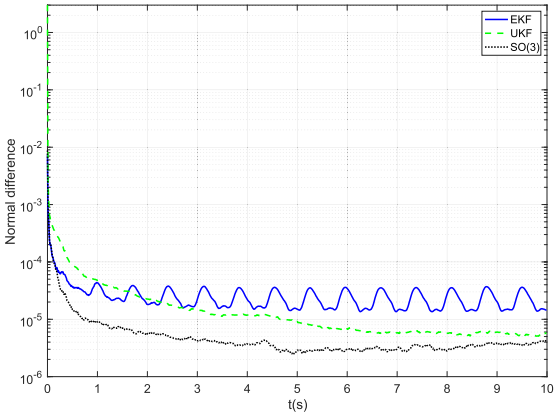

FIGURE 10. Frobenius norm of the EKF, UKF and $\mathcal{SO}(3)$ rotation matrices at 1000Hz.

the Kalman filters will introduce additional uncertainty due to the linearization process, when compared to the $\mathcal{SO}(3)$ tracker. The Frobenius norm values for the $\mathcal{SO}(3)$ tracker (from Equation (31)) are small throughout and do not accumulate over time. From the progression of Figures 4 to 7 and then 10, it is clear that the performance of EKF and UKF becomes more and more comparable with the $\mathcal{SO}(3)$ as the sampling rate increases. This coincides with the theoretical property of the Kalman filters, in which the local linearization improves due to the shorter intervals between measurements. Additionally, we can see that the $\mathcal{SO}(3)$'s performance is improved accordingly. Our simulations at 10Hz exemplify the difference in the approaches in attitude estimation using low-cost sensors. Best visualised in Fig. 2 and Fig. 4, the EKF struggles in the initialisation and starts drifting almost immediately. In contrast, we see that both the UKF and $\mathcal{SO}(3)$ remain constant throughout. However the $\mathcal{SO}(3)$ converges much more quickly and provides a more accurate estimation. In summary, when our measurement frequency is $f = 1000$Hz, the performance of all trackers are reasonably close to each other but when $f = 10$Hz, the performance of $\mathcal{SO}(3)$ is a significantly better solution. It is important to note that despite each of the Kalman approaches convergence to a more comparable solution as the sampling time increases, the $\mathcal{SO}(3)$ still remains superior.

B. ATTITUDE ESTIMATION: REAL DATA

The *OXIOD* dataset is a publicly available at [12] and aims to reproduce everyday activities using off-the-shelf consumer phones and Motion Capture as a means of ground truth. The dataset contains 158 sequences totalling more than 42km in total distance. The data collection was designed to best represent the varying complexity of motions of phone-based IMUs in everyday usage, utilising four different off-the-shelf consumer phones and five different users. The scenarios in the dataset describe the user over three different motion modes: slow walking, walking at a regular pace and running - all with phone in hand. Further scenarios have the user walking at a regular pace with the phone in a handbag, pocket or trolley. We have compared each approach over each scenario, using error variance as our performance metric, for each Euler angle. The variance is given by:

$$\sigma^2 = \frac{\sum_{i=1}^{n}(\alpha_k - \overline{\alpha})^2}{n-1} \tag{32}$$

where α_k is the estimate error at point k, $\overline{\alpha}$ is the mean error and n is the number of estimates.

By leveraging the true attitude representations using the genetic algorithm [30], we were able to calculate optimal covariance parameters for each filter to evaluate their situational best-case solution. Our results are presented in Figures 11-13.

In Figure 11, the variance for the Euler *pitch* estimate is given for each approach and activity. Given the results in Section VI-A, it would follow that the $\mathcal{SO}(3)$ and UKF produce comparable solutions and the EKF trails with a larger variance. It can be seen that this is largely the case, with an exception when the phone was placed in the pocket of the user. This is possibly due to the EKF having the chance to reinitialise when the device aligned with the gravitational vector. The variance of our *roll* estimates (in Figure 12) are even more in-line with our theoretical expectations and

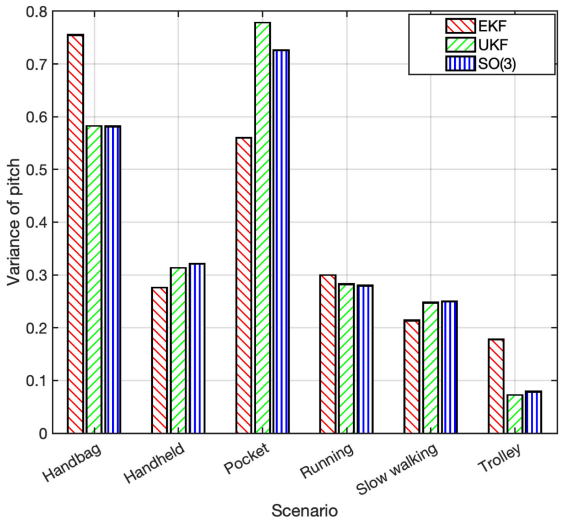

FIGURE 11. Variance of pitch obtained from the EKF, UKF and $\mathcal{SO}(3)$, for each aggregated scenario in the OXIOD dataset.

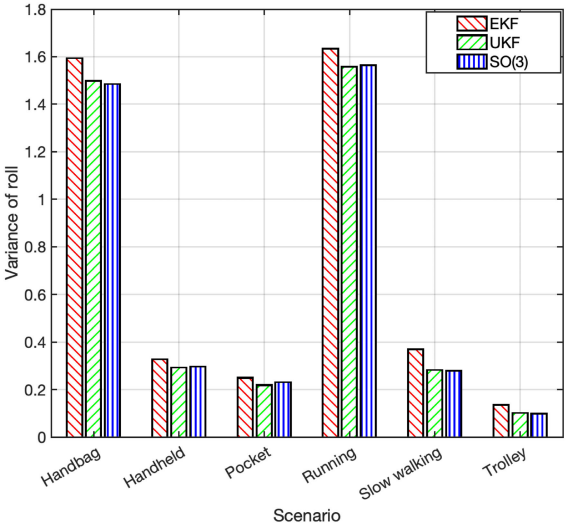

FIGURE 12. Variance of roll obtained from the EKF, UKF and $\mathcal{SO}(3)$, for each aggregated scenario in the OXIOD dataset.

simulated results, where we see the $\mathcal{SO}(3)$ perform best, followed closely by the UKF and then the EKF. Again, in Figure 13, the *yaw* estimates mirror those from our Monte Carlo simulations, in which the $\mathcal{SO}(3)$ tracker significantly outperforms the Kalman variants.

We can numerically quantify the robustness of each approach by looking at the mean variance over the entire dataset. The mean variance of the pitch estimates for the EKF, UKF and $\mathcal{SO}(3)$ are 0.38, 0.38, 0.37 respectively. Roll mean variances 0.72, 0.65, 0.65 and finally yaw, 2.34, 1.27, 0.93. Averaging over these results for each approach gives 1.15, 0.77, 0.65 for the EKF, UKF and $\mathcal{SO}(3)$, respectively. It is evident from these measures that $\mathcal{SO}(3)$ outperforms the Kalman filters, with significant improvement in yaw estimation in particular. With an exception noted in the scenarios where the phone was placed in the pocket of the user, where we see the EKF compute a better pitch estimate.

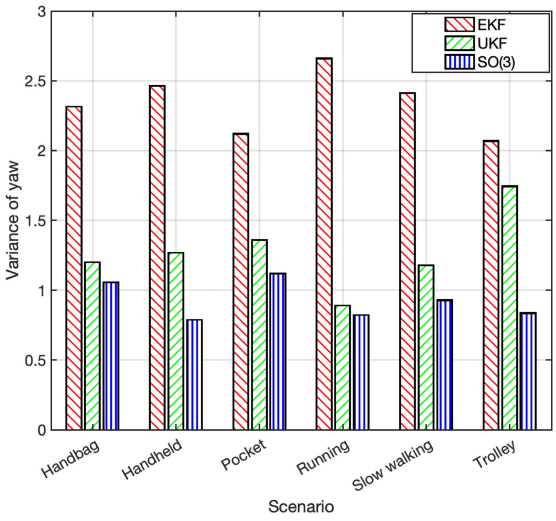

FIGURE 13. Variance of yaw obtained from the EKF, UKF and $\mathcal{SO}(3)$, for each aggregated scenario in the OXIOD dataset.

TABLE 1. Computation comparison.

	EKF	UKF	$\mathcal{SO}(3)$
Rot. gen per sec	13848	213	416
Ratio to best	1	65.09	30.26

C. PROCESSING TIME

Since battery saving is a crucial component in a smartphone, processing time is paramount to its applicability. Table 1 reports the number of rotation matrices generated per second using Matlab. The larger the number, the better the performance of the algorithm. Computationally, the EKF outperforms the $\mathcal{SO}(3)$ and UKF. The second line indicates the ratio of the time spent in each algorithm compared to the EKF.

Overall, in our experimental setting, we observe that each algorithm can be executed on smartphones at 100Hz. It is also of special interest to note that in cases where battery life is of particular importance, the ability of the $\mathcal{SO}(3)$ to sample less frequently than the Kalman algorithms without sacrificing much accuracy could allow for further power reductions. However this will need to be further investigated.

VII. CONCLUSION

In this work, we have evaluated popular attitude estimation algorithms: the traditional Extended Kalman filter and Unscented Kalman filter and using maximal entropy distributions on the rotation group $\mathcal{SO}(3)$. We tested their performance using simulated IMU measurements, emulated from a typical smartphone over varying frequencies, and a large, publicly available dataset. We showed that the $\mathcal{SO}(3)$

outperforms the EKF and UKF estimations under most test conditions, with the largest discrepancies coming from low rate sensor data and yaw estimation. It is well known that the EKF is a sub-optimal and biased estimator due to the errors introduced in the linearization and the resultant calculation of the Jacobian. We showed that both Kalman variants are more sensitive to the change of sampling rate than the $\mathcal{SO}(3)$ tracker, due to the different modelling methods. Our evaluations on the real dataset prove the $\mathcal{SO}(3)$ filter is not only a better estimate solution, but also more robust. Adoption of the $\mathcal{SO}(3)$ filter to process inertial measurements for attitude estimation in smartphones could improve not only attitude reliant applications such as augmented/virtual reality and navigation, but also improve battery life due to its ability to produce accurate estimations at reduced sampling intervals. We look to improve on this solution and future work will aim to optimise the mean and covariance estimates in the $\mathcal{SO}(3)$ filter, as well as reformulating gyroscope bias estimation with sigma point or particle estimation.

REFERENCES

[1] J. González-García, A. Gómez-Espinosa, E. Cuan-Urquizo, L. G. García-Valdovinos, T. Salgado-Jiménez, and J. A. E. Cabello, "Autonomous underwater vehicles: Localization, navigation, and communication for collaborative missions," *Appl. Sci.*, vol. 10, no. 4, p. 1256, Feb. 2020.

[2] E. J. Lefferts, F. L. Markley, and M. D. Shuster, "Kalman filtering for spacecraft attitude estimation," *J. Guid., Control, Dyn.*, vol. 5, no. 5, pp. 417–429, 1982.

[3] B. Liu, Z. Chen, X. Liu, and F. Yang, "An efficient nonlinear filter for spacecraft attitude estimation," *Int. J. Aerosp. Eng.*, vol. 2014, pp. 1–11, Jan. 2014.

[4] X. Wang, S. Suvorova, T. Vaithianathan, and C. Leckie, "Using trajectory features for upper limb action recognition," in *Proc. IEEE 9th Int. Conf. Intell. Sensors, Sensor Netw. Inf. Process. (ISSNIP)*, Apr. 2014, pp. 1–6.

[5] J. L. Crassidis, F. L. Markley, and Y. Cheng, "Survey of nonlinear attitude estimation methods," *J. Guid., Control, Dyn.*, vol. 30, no. 1, pp. 12–28, 2007.

[6] F. Daum, "Nonlinear filters: Beyond the Kalman filter," *IEEE Aerosp. Electron. Syst. Mag.*, vol. 20, no. 8, pp. 57–69, Aug. 2005.

[7] T. Lee, "Bayesian attitude estimation with the matrix Fisher distribution on SO(3)," *IEEE Trans. Autom. Control*, vol. 63, no. 10, pp. 3377–3392, Oct. 2018.

[8] T. Michel, H. Fourati, P. Geneves, and N. Layaïda, "A comparative analysis of attitude estimation for pedestrian navigation with smartphones," in *Proc. Int. Conf. Indoor Positioning Indoor Navigat. (IPIN)*, Oct. 2015, pp. 1–10.

[9] T. Michel, P. Geneves, H. Fourati, and N. Layaïda, "On attitude estimation with smartphones," in *Proc. IEEE Int. Conf. Pervasive Comput. Commun. (PerCom)*, Mar. 2017, pp. 267–275.

[10] H. Chao, C. Coopmans, L. Di, and Y. Chen, "A comparative evaluation of low-cost IMUs for unmanned autonomous systems," in *Proc. IEEE Conf. Multisensor Fusion Integr.*, Sep. 2010, pp. 211–216.

[11] S. Suvorova, S. D. Howard, and B. Moran, "Tracking rotations using maximum entropy distributions," *IEEE Trans. Aerosp. Electron. Syst.*, vol. 57, no. 5, pp. 2953–2968, Oct. 2021.

[12] C. Chen, P. Zhao, C. Xiaoxuan Lu, W. Wang, A. Markham, and N. Trigoni, "OxIOD: The dataset for deep inertial odometry," 2018, *arXiv:1809.07491*.

[13] C. R. Ehrlich and J. Blankenbach, "Indoor localization for pedestrians with real-time capability using multi-sensor smartphones," *Geo-Spatial Inf. Sci.*, vol. 22, no. 2, pp. 73–88, Apr. 2019.

[14] L. Perea, J. How, L. Breger, and P. Elosegui, "Nonlinearity in sensor fusion: Divergence issues in EKF, modified truncated GSF, and UKF," in *Proc. AIAA Guid., Navigat. Control Conf. Exhib.*, Aug. 2007, p. 6514.

[15] X. Tang, J. Yan, and D. Zhong, "Square-root sigma-point Kalman filtering for spacecraft relative navigation," *Acta Astronautica*, vol. 66, nos. 5–6, pp. 704–713, Mar. 2010.

[16] Y.-S. Suh, S.-K. Park, H.-J. Kang, and Y.-S. Ro, "Attitude estimation adaptively compensating external acceleration," *Int. J. C Mech. Syst., Mach. Elements Manuf.*, vol. 49, no. 1, pp. 172–179, 2006.

[17] S. Y. Cho and W. S. Choi, "Robust positioning technique in low-cost DR/GPS for land navigation," *IEEE Trans. Instrum. Meas.*, vol. 55, no. 4, pp. 1132–1142, Aug. 2006.

[18] S. J. Julier and J. K. Uhlmann, "New extension of the Kalman filter to nonlinear systems," *Proc. SPIE*, vol. 3068, pp. 182–193, Apr. 1997.

[19] J. L. Crassidis and F. L. Markley, "Unscented filtering for spacecraft attitude estimation," *J. Guid., Control, Dyn.*, vol. 26, no. 4, pp. 536–542, Jul. 2003.

[20] J.-B. Lacambre, M. Narozny, and J.-M. Louge, "Limitations of the unscented Kalman filter for the attitude determination on an inertial navigation system," in *Proc. IEEE Digit. Signal Process. Signal Process. Educ. Meeting (DSP/SPE)*, Aug. 2013, pp. 187–192.

[21] C. G. Khatri and K. V. Mardia, "The von Mises–Fisher matrix distribution in orientation statistics," *J. Roy. Stat. Soc. B, Methodol.*, vol. 39, no. 1, pp. 95–106, 1977.

[22] P. E. Jupp and K. V. Mardia, "Maximum likelihood estimators for the matrix von mises-Fisher and Bingham distributions," *Ann. Statist.*, vol. 7, no. 3, pp. 599–606, May 1979.

[23] S. Suvorova, S. Howard, and B. Moran, "Bayesian recursive estimation on the rotation group," in *Proc. IEEE Int. Conf. Acoust., Speech Signal Process.*, May 2013, pp. 6411–6415.

[24] J. T.-H. Lo and L. R. Eshleman, "Exponential Fourier densities on SO(3) and optimal estimation and detection for rotational processes," *SIAM J. Appl. Math.*, vol. 36, no. 1, pp. 73–82, 1979.

[25] I. V. L. Clarkson, S. D. Howard, W. Moran, D. Cochran, and M. L. Dawson, "Maximum-likelihood and best invariant orientation estimation," in *Proc. 44th Asilomar Conf. Signals, Syst. Comput.*, Nov. 2010, pp. 1996–2000.

[26] P. Hargrave, "A tutorial introduction to Kalman filtering," in *Proc. IEE Colloq. Kalman Filters, Introduction, Appl. Future Develop.*, Feb. 1989, p. 1.

[27] A. C. B. Chiella, B. O. S. Teixeira, and G. A. S. Pereira, "Quaternion-based robust attitude estimation using an adaptive unscented Kalman filter," *Sensors*, vol. 19, no. 10, p. 2372, May 2019.

[28] A. C. B. Chiella, B. O. S. Teixeira, and G. A. S. Pereira, "Quaternion-based robust attitude estimation using an adaptive unscented Kalman filter," *Sensors*, vol. 19, no. 10, p. 2372, May 2019.

[29] A. Kos, S. Tomažič, and A. Umek, "Evaluation of smartphone inertial sensor performance for cross-platform mobile applications," *Sensors*, vol. 16, no. 4, p. 477, 2016.

[30] K. L. Shi, T. F. Chan, Y. K. Wong, and S. L. Ho, "Speed estimation of an induction motor drive using an optimized extended Kalman filter," *IEEE Trans. Ind. Electron.*, vol. 49, no. 1, pp. 124–133, Feb. 2002.

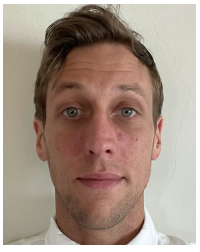

JAMES BROTCHIE received the B.S. degree in physics from RMIT University, Melbourne, Australia, in 2016, with a research focus on blind quantum protocols in measurement-based quantum computing, where he is currently pursuing the Ph.D. degree in geospatial science. From 2016 to 2018, he was a Research Assistant with the Department of Optometry and Vision Sciences and the Victorian Department of Health and Human Services, The University of Melbourne, Australia, where his focus was statistical parametric mapping. In 2021, he joined Institec Pty Ltd., as the Technical Lead in geospatial research and development. His research interests include sensor fusion, object tracking, statistical analysis, and modeling.

WENCHAO LI received the B.S. and M.S. degrees in control theory from the Xi'an University of Technology, Xi'an, China, in 2005 and 2008, respectively, and the Ph.D. degree in electronic engineering from The University of Melbourne, Melbourne, Australia, in 2018. He is currently a Research Fellow with RMIT University. His research interests include statistical signal processing and number theory with applications in sensor networks, including range estimation, resolving phase ambiguity, and sensor localization.

ALLISON KEALY received the B.S. degree in land surveying from The University of the West Indies, Trinidad, and the Ph.D. degree in satellite positioning and geodesy from the University of Newcastle, Newcastle upon Tyne, U.K. He is currently a Professor in geospatial science with RMIT University, Australia. He is also the Research Director, Program 2, Advanced Satellite Systems, Sensors and Intelligence, SmartSAT CRC, the President of the International Association of Geodesy (IAG) Commission 4—Positioning and Applications, the Deputy Director of the Sir Lawrence Wackett Centre for Defence Research with RMIT University and a Technical Representative on the U.S. Institute of Navigation Council. His multi-disciplinary research extends across high performance PNT applications, GNSS quality control, sensor fusion, and estimation theory.

BILL MORAN (Member, IEEE) received the B.S. degree (Hons.) in mathematics from the University of Birmingham, in 1965, and the Ph.D. degree in pure mathematics from the University of Sheffield, U.K., in 1968. He was the Director of the Signal Processing and Sensor Control Group, School of Engineering, RMIT University, from 2001 to 2014, a Professor with the Department of Electrical Engineering, The University of Melbourne, where he was the Director of the Defence Science Institute, from 2011 to 2014, a Professor in mathematics, from 1976 to 1991, the Head of the Department of Pure Mathematics, from 1977 to 1979, and, from 1984 to 1986, the Dean of Mathematical and Computer Sciences, in 1981, 1982, and 1989, with the University of Adelaide, and the Head of the Mathematics Discipline with the Flinders University of South Australia, from 1991 to 1995. He was the Head of the Medical Signal Processing Program with the Cooperative Research Centre for Sensor Signal and Information Processing, from 1995 to 1999. He has been working, since 2017, as a Professor of Defence Technology with The University of Melbourne. His research interests include signal processing both theoretically and in applications to radar, waveform design and radar theory, sensor networks, and sensor management. He also works in various areas of mathematics, including harmonic analysis, representation theory, and number theory.